Development and Analysis of an Autorotating, Disposable Micro Air Vehicle for Tactical Surveillance

Benjamin Thomas Flood[1]

University of New South Wales at the Australian Defence Force Academy

The aim of this project was to further investigate the feasibility of a gas-gun-launched, disposable Micro Air Vehicle (MAV) for use in tactical situations. The MAV, once propelled to altitude by a gas powered initiator, utilises autorotation to reduce its terminal descent rate while inbuilt cameras capture the tactical situation below. The concept has the potential to greatly benefit ground forces in suburban areas by providing them with an instantaneous, fire and forget source of enhanced battle-field awareness. This project focused on the optimisation of the rotor blades for the MAV, particularly through blade twist. Vertical autorotation performance has been analysed by both computational and experimental methods; a MATLAB model founded on Blade Element Momentum Theory has been written and low turbulence wind tunnel experimentation has been conducted. The experimental results have shown that the terminal descent velocity of the MAV could be substantially reduced through the implementation of positive linear blade twist between 11º and 19.5º. The computational analysis produced has been proven to identify performance variation due to blade twist however was unable to recognise the peaks in performance identified by the experimental analysis. As such the MATLAB model will require further development before being utilised for future autorotation analysis and optimisation.

Contents

[1] Sub Lieutenant, Undergraduate, School of Engineering & Information Technology, UNSW@ADFA

Nomenclature

α	=	angle of attack [°]
BET	=	Blade Element Theory
BEMT	=	Blade Element Momentum Theory
c	=	chord [m]
C_d	=	coefficient of drag
C_l	=	coefficient of lift
$C_{l\alpha}$	=	lift curve slope
dD	=	elemental drag force [N]
dF	=	elemental net force [N]
dL	=	elemental lift force [N]
dT	=	elemental thrust [N]
dQ	=	elemental torque [N•m]
GLMAV	=	Gun Launched Micro Air Vehicle
L	=	lift force [N]
m	=	mass [kg]
MAV	=	Micro Air Vehicle
μ	=	viscosity coefficient
Ω	=	angular velocity [radians•s^{-1}]
φ	=	inflow angle [radians]
Q	=	total shaft torque [N•m]
r	=	elemental radius [m)
R_i	=	radius of blade root [m]
R	=	rotor disk radius [m]
RPM	=	revolutions per minute
ρ	=	air density [kgm^{-3})
SEIT	=	School of Engineering and Information Technology
SUAV	=	Small Unmanned Aerial Vehicle
T	=	total rotor thrust
UAV	=	Unmanned Aerial Vehicle
UNSW	=	University of New South Wales
V_c	=	climb velocity [ms^{-1}]
V_d	=	descent velocity [ms^{-1}]
V_i	=	induced velocity [ms^{-1}]
V_r	=	incident velocity [ms^{-1}]
V_x	=	horizontal component incident airflow [ms^{-1}]
V_y	=	vertical component of incident airflow [ms^{-1}]
VRS	=	Vortex Ring State
x	=	subscript, indicates horizontal plane
y	=	subscript, indicates vertical plane

I. Introduction

THIS report focuses on the reduction of the terminal descent rate for an autorotating MAV through the application of blade twist. Computational and experimental analysis has been used to quantify the effect of linear blade twist on steady state autorotation and hence allow the optimisation of the MAV rotor blades. This work allows the MAV to remain airborne for a greater period of time and consequently provide greater quantities of information to ground forces in tactical situations.

A. Background

Figure 1. Black Hornet MAV

The advent of UAVs has changed the way that surface warfare is fought. Ground forces now have an increased situational awareness of their conflict environment due to a range of sensor equipped UAVs being available to provide up to date information regarding enemy movements and landscape [28]. This has significantly reduced the risks involved for ground forces as they are now able to see the environment they intend to enter, before they enter it [20]. The importance of UAV technology has increased significantly as the modern battlefield has moved away from traditional field warfare and into the urban environment. Large scale UAVs such as the Global Hawk and Predator are able to provide airborne surveillance to ground forces for up 24 hours at a time [1,11]. However if the requirement is not anticipated the ground forces will be without UAV provided intelligence until an aircraft becomes available and makes its way to their location. For this reason smaller scale UAVs, like the trailer transported and launched RQ-7 Shadow, have been developed in order to provide ground forces with greater self-sufficiency. The next step in developing self-sufficiency is to provide a UAV capability to foot-soldiers. Currently there are a number of SUAVs in operation; the RQ-11 Raven and RQ-14 Dragon Eye. Both of these aircraft are fixed wing UAVs with wingspans of 1.4 m and 1.1 m respectively [2,31]. While they can be carried in a backpack, these aircraft significantly reduce the amount of other mission essential equipment a soldier can carry. The need for lower weight and volume resulted in the development of the Wasp (72 cm wingspan), the Black Widow (15 cm wingspan) and the rotary winged Black Hornet (10 cm fuselage length) as seen in Fig.1 [3,8,10]. These aircraft are all capable of flight times in excess of 20 minutes under either remote control or GPS waypoint navigation [29], however they are expensive; a single Black Hornet system comes at a cost of $195,000 US. These MAVs also require either a considerable amount of set up time if they are to be flown by GPS waypoints, or the constant attention of an operator if being flown by remote control. While these systems provide a valuable capability they require an operator with significant levels of training to operate them, and, although faster to respond than a large scale UAV, these systems still take a significant amount of time to be positioned over a desired target.

In 2012 Power [25] conducted a feasibility study into the concept of a gas-gun launched, disposable, autorotating MAV named Falling Spy. He concluded that a small projectile (52x150 mm) could be fired by a gas gun, known as the Initiator, to an altitude at which it would deploy rotor blades and descend under autorotation while a base mounted camera would capture the situation below. The system has the potential to provide a much shorter response time than alternative MAVs by reducing the time required for set-up and the time to target. Falling Spy is also intended to be simple to use, meaning that any member in a fighting force could operate it with limited training, unlike alternate MAVs which require specific training likely to be delivered only to select members of a fighting force. The use of a gas-gun rather than conventional deployment system was chosen due to its low visual and audible signal. The decision to use autorotation instead of a parachute was made in order reduce the MAV's visual signature and hence make it less vulnerable to attack, the subsequent reduction in surface area also makes the MAV less affected by crosswind and will hence be more inclined to descend directly over its intended target. As the MAV is intended to be disposable the cost of the final design will have to be kept to a minimum in order to compete against reusable MAVs, a result of this is that a primary design objective is for the MAV's flight to be as passive as possible.

B. Autorotation and the Importance of Blade Twist

As this project will focus on the optimisation of the autorotation performance of the MAV the theory behind autorotation must first be understood. Autorotation has been utilised by nature for thousands of year for the dispersal of samara fruit and seeds however, the term is now conventionally used in reference to the recovery technique used by helicopter pilots in the event of power failure [7]. At the point of power failure the pilot is able to maintain rotor speed by reducing the positive collective pitch. As the helicopter descends the upward flow of air continues to drive the rotor blades allowing lift to be produced even without power, slowing the rate of descent of the aircraft.

During autorotation the rotor blades are divided into three distinct sections as displayed by Fig.2; the stalled, driving and driven regions [14,17].

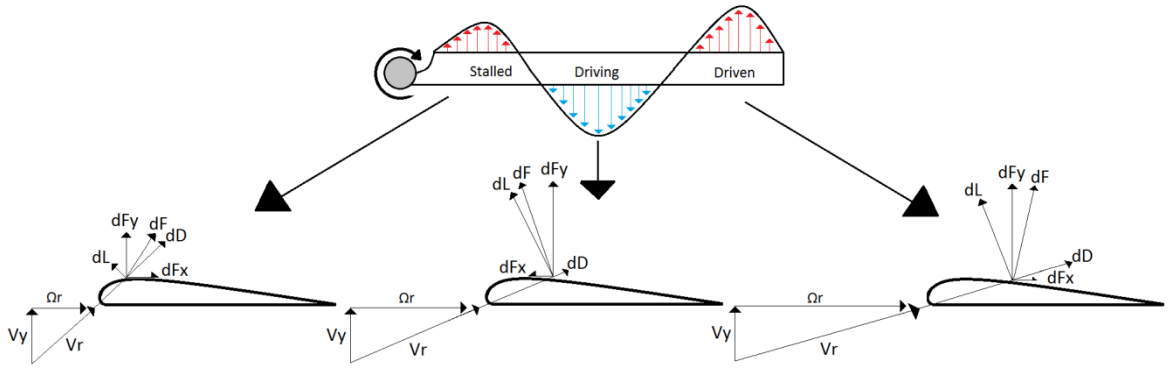

Figure 2. Blade Regions during Autorotation

Across the rotor disc radius the vertical flow the blades encounter is relatively constant however as the disc is rotating the horizontal airflow the blades encounter increases in magnitude with radius. The result is an inflow angle, φ, which decreases toward the tips of the blades. In the driving region of the blade the inflow angle will be such that the lift x-component of the lift produced will be greater than the x-component of the produced drag. This results in a net horizontal force which accelerates the rotor disc's rotation. As the inflow angle reduces toward the tip the lift force becomes more vertical and the drag becomes the more dominant horizontal force, which decelerates the rotor disc's rotation. This is known as the driven region and is where most of the rotor disc's thrust is produced[14,17]. Toward the roots of the blades the inflow angle is so great that the blades become stalled. This region of the blade produces very little lift but a considerable amount of drag, resulting in slowed rotation of the rotor disc and a higher descent rate.

It was hypothesised that passive autorotation performance could be improved by applying a small amount of linear blade twist and subsequently reducing the size of the stalled region and increasing the efficiency of the driven region. The rotor disc on a traditional helicopter operates with a positive collective pitch as the airflow during conventional flight flows in from the top of the rotor disc. The blades are typically designed with a negative blade twist in order to reduce the geometric pitch at the tips of the blades. However, during passive autorotation the airflow is received by the rotor disc from below and as such it is necessary to have a negative collective pitch in order to initiate rotation, more akin to a wind turbine than a conventional helicopter. Consequently a positive blade twist is required to reduce the magnitude of the geometric pitch at the blade tips.

C. Previous Work Conducted on Project Falling Spy

In 2013 Kelderman and Rolph followed on from Power [15,27]. Rolph focussed primarily on the design and testing of the Initiator, the further development of which is currently being conducted by Stockdale [30]. Rolph's work recommended that further investigation be conducted with regard to the development of the MAV, specifically its blade and geometric design. Kelderman followed on from Power's work by focussing primarily on the design of the MAV's rotor blades using both computational analysis and drop testing.

Kelderman's computational analysis used the basic autorotation calculations used by Power to analyse the effects of blade characteristics on the autorotation descent velocity of the MAV. Kelderman's findings show that the descent velocity was affected by blade chord, rotor disc radius, MAV mass and collective pitch in the following ways:

$$V_y \propto \frac{1}{\sqrt{c}}, \quad V_y \propto \frac{1}{\sqrt{r}}, \quad V_y \propto \sqrt{m}, \quad V_y \propto f(collective\ pitch)$$

D. Work Conducted on Similar Projects

Gnemmi & Haertig proposed a similar MAV in 2008 [9]. Unlike the MAV proposed for Falling Spy, Gnemmi and Haertig's GLMAV was to be an active MAV. Once fired, the GLMAV utilises two powered contra-rotating sets of rotor blades to remain airborne for up to 20 minutes under either remote control or autonomous GPS navigation as shown in Fig.3. Due to its active flight characteristics the GLMAV is not disposable and returns to its operator once its flight has competed. The GLMAV was designed with a blade twist of -6.945°/m.

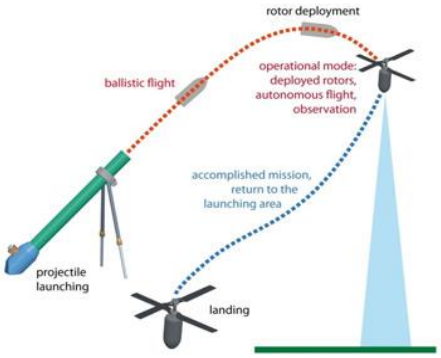

Figure 3. GLMAV

Murphy & Mullen propose a model more relevant to this particular project [21]. Their ACSDS, as shown in Figure 4. ACSDS incorporates the use of autorotation to provide a controlled descent of electronic sensors into jungle canopies, for the purpose of intelligence gathering during conflict in low-latitude environments. The ACSDS is designed to be released from an aircraft and descend silently until it is captured by the jungle canopy where it collects and transmits information through a variety of sensors embedded in its 24 in, 3 lb payload. The ACSDS, like the Falling Spy MAV has been designed for vertical, passive autorotation. Murphy & Mullen note that blade twist is an important design feature of blades designed for autorotation however they do not discuss the matter further.

Figure 4. ACSDS

Brindejonc *et al* conducted a more in depth analysis of the ACSDS's rotor blades focussing specifically on the pitch-flap coupling angle, collective pitch and coning angle [4]. The study conducted involved two phases, a computational model and a series of wind tunnel tests. The computational model used a method called RPM Sweep to analyse the effects of blade characteristics on autorotation performance through BEMT. This computational analysis was then verified through a series of wind tunnel tests. Importantly both the computational and experimental methods produced a quadratic relationship between thrust produced and the descent velocity and a linear relationship between the RPM and descent velocity. Brindejonc *et al*. concluded that the pitch flap coupling angle, collective pitch and precone angle are optimum at values of -41°, -10° and -4° respectively. The analysis resulted in a prototype's construction. The prototype was designed with blade tip twist of +7.75° in order to gain a more uniform lift distribution along the blade length. The reasoning behind the selection of this value is not explained however it is noted by Brindejonc *et al*. that in order to initiate autorotation in the desired direction the blade pitch must be negative at three quarters of the blade radius.

II. Investigation and Analysis

A. Blade Element Momentum Theory

Commonly there are two computational methods for analysing helicopter performance, Blade Element Theory and Momentum Theory [4,14,17].

Blade Element Theory mathematically breaks a rotor blade into small elements along its length as shown in Fig.5. Each of these elements is then treated as an independent two dimensional airfoil to gain an understanding of the aerodynamic conditions it is under and subsequently the aerodynamic forces that it produces are calculated in accordance with Fig.6 and the following equations [4, 12, 14, 17, 18,19].

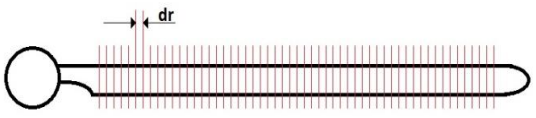

Figure 5. Blade Elements

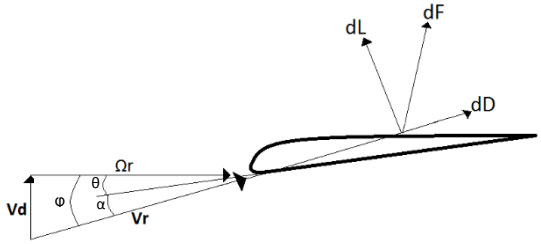

Figure 6. BET Airfoil Dynamics for Autorotation

$$V_y = V_d \quad (1)$$

$$V_r = \sqrt{V_y^2 + \Omega^2 r^2} \quad (2)$$

$$\varphi = \tan^{-1}\frac{V_y}{\Omega r} \quad (3)$$

$$\alpha = \varphi - \theta \quad (4)$$

$$C_l = C_{l\alpha}\varphi \quad (5)$$

$$C_d = C_{d\alpha}\varphi \quad (6)$$

$$dL = \frac{1}{2}\rho V_r^2 C_l c dr \quad (7)$$

$$dD = \frac{1}{2}\rho V_r^2 C_d c dr \quad (8)$$

$$dT = dL\cos\varphi + dD\sin\varphi \quad (9)$$

$$dQ = (dL\sin\varphi - dD\cos\varphi) \times r \quad (10)$$

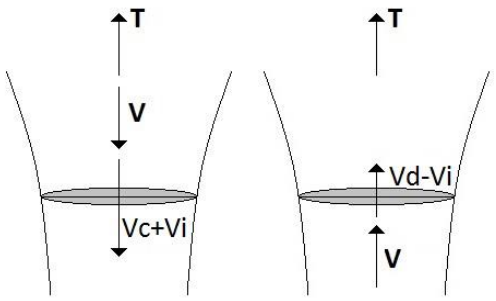

Figure 7. Momentum Theory in Normal Working State (a) and Autorotation (b)

Once each element has been analysed the forces are combined to gain values for the entire rotor.

$$T = N\sum_{Ri}^{R} dT \quad (11)$$

$$Q = N\sum_{Ri}^{R} dQ \quad (12)$$

Momentum Theory treats the entire rotor disk as an actuator disk as show in Fig.7 which induces a velocity, V_i, to the air flowing through it. The thrust is then calculated using the following equation:

$$T = 2\rho A V_i^2 \quad (13)$$

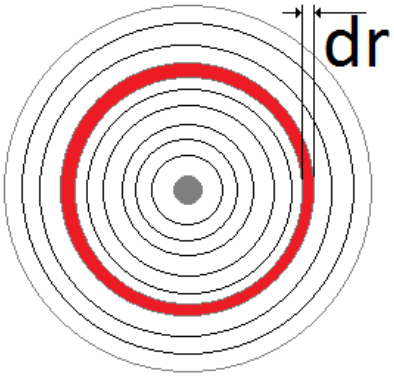

Figure 8. Rotor Annuli for BEMT

Blade Element Momentum Theory combines Blade Element Theory and Momentum Theory to produce a more accurate analysis of helicopter performance. For each blade element aerodynamic conditions and resultant forces are calculated. The elemental thrust is then multiplied by the number of blades to find the amount of thrust for its coinciding annulus as shown in Fig.8.

$$dT = N \times (dL\cos\varphi + dD\sin\varphi) \quad (14)$$

The area of the annulus is then substituted into Eq.13 which is then rearranged Eq.15 and then used to calculate the induced velocity.

$$V_i = \sqrt{\frac{dT}{2\rho\pi\left(\left(r+\frac{dr}{2}\right)^2 - \left(r-\frac{dr}{2}\right)^2\right)}} \quad (15)$$

From V_i, V_y is recalculated and the process is repeated until convergence is achieved. Unlike a helicopter in normal working state where the inflow and induced velocity are both directed down through the rotor disc, autorotation sees the inflow entering the rotor disc from below, thus it is necessary to subtract the induced velocity from the descent velocity.

$$V_y = V_d - V_i \quad (16)$$

B. Computational Analysis Design

The computational analysis developed for this project used RPM Sweep and BEMT to calculate the thrust produced by individual blade configurations over an array of descent velocities as shown in Fig.9. RPM Sweep operates by setting the descent velocity and selecting a RPM value, BEMT is then used to calculate the net thrust and torque of the rotor disc before a new RPM value is tested. This is repeated until the RPM value that produces zero net torque is found, the coinciding net thrust is then recorded as the value which is achieved at the selected descent rate. This process is then repeated over a range of descent velocities for each of the blade configurations to be analysed

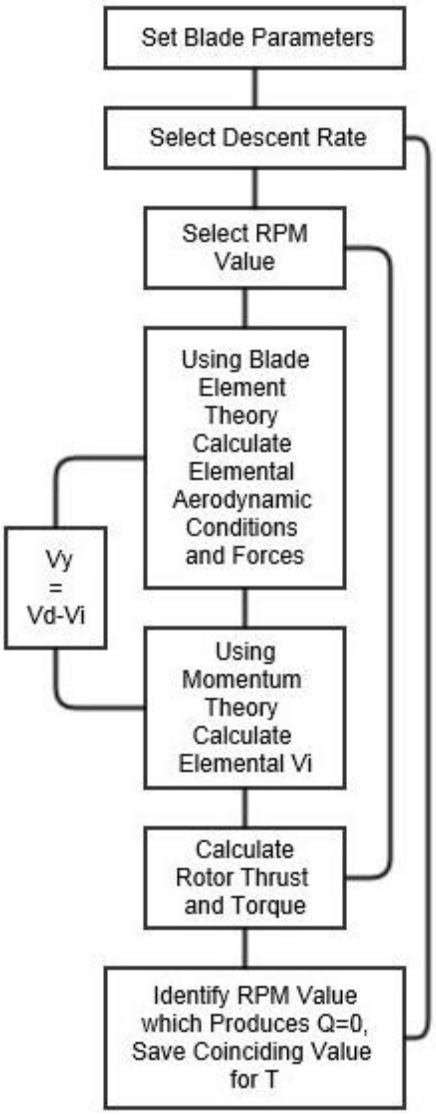

Figure 9. BEMT and RPM Sweep Computation Flow Chart

C. Experiment Design

Experiments were conducted using the UNSW SEIT Low Turbulence Wind Tunnel in order to verify the results produced by the computational analysis.

The wind tunnel model was designed and built with the intent to provide a system which provided accurate and repeatable variations in both collective pitch and blade twist while maintaining minimal rotational resistance. As this project focuses on eventually producing a compact MAV the blade root radius was to be kept as small as possible. The resultant design was an all spinning 3D printed fuselage which housed four 53 mm servo arms as shown in Fig.10. The servo arms provided a 25 tooth splined hub which allowed the blade grips to be mounted at five distinct and repeatable collective pitches. The blade grips, which were designed around a 25 tooth splined shaft used grub screws to allow simple and accurate replacement of the blades. The full blade grip assembly is shown in Fig.11. The blades were constructed from 20 x 1.6 mm aluminium flat bar. As the material chosen for the blades was not cambered, flat plate calculations for coefficients of lift and drag could be used in the computational analysis. Linear twist was applied to the blades using a Gunt WP510 Torsion Testing Apparatus with an accuracy of ±0.5º.

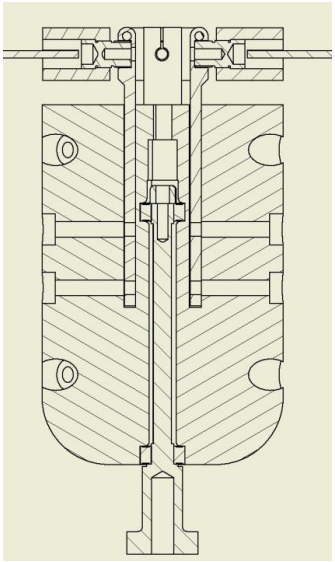

Figure 10. Wind Tunnel Model Cross Section

Figure 11. Wind Tunnel Model Blade Grip Assembly

The windspeed of the tunnel was measured using a commercial anemometer as a calibrated micromanometer was not available. For the results of the experiments to be considered truly valid the anemometer used would have to be compared to a calibrated instrument and the results adapted accordingly. Without the means to verify the anemometer's readings the wind speed data was assumed to be within ±0.05 ms^{-1} of actual values.

Figure 12. Wind Tunnel Experiment Set-up

The rotation rate of the model was measured using both a variable frequency strobe light and a Hioki laser tachometer. The strobe light which was calibrated using a photo detector and oscilloscope was aimed at the model and its frequency varied until the model appeared to no longer be rotating. The frequency displayed on the strobe light was then deemed to be that of the model's rotation. After conducting a number of tests it was found that the strobe technique was excessively time consuming. A Hioki laser tachometer was then implemented as it was able to take readings in a much faster manner. Once a reflective strip had been applied to the wind tunnel model the tachometer was able to quickly and accurately produce the model's RPM on its digital display. Initially these readings were verified with the strobe light however once the tachometer was deemed to be producing accurate results it was used independently.

The thrust of the wind tunnel model was measured using a force balance, HP 75000 Computer and HPVEE Software. The force balance was calibrated using a series of calibrated weights to develop a conversion matrix for the raw data that the force balance strain gauges produced. The conversion matrix accounts for the cross coupling of forces experience by the strain gauges and produces the pitch, lift and drag forces applied to the sting which holds the wind tunnel model in the airflow [16,23,24,26]. The Wind Tunnel Experimental Set-up including the wind tunnel model, anemometer and force balance is shown in Fig.12.

D. Wind Tunnel Experimentation and Results

Initially the wind tunnel model was tested using only a 2 mm clamp screws, which simply tightened the fit of the splined components, to hold the blade grips in the servo arms. At approximately 1100 RPM the centrifugal force caused one of the blade grips to detach from its servo arm. The instantaneous imbalance of the system at high speed caused the central shaft to bend, resulting in delays to testing as it was repaired. Subsequently the clamping screws were replaced by 3 mm cap screws which passed through the servo arms into threads in the blade grips in order to directly fasten the splined shafts into the servo arms. Further a 700 RPM ceiling was placed on the apparatus to prevent further damage to the central shaft until an initial set of data had been acquired.

The first series of testing saw six blade twists; 0º, 11º, 16º, 19.5º, 25º, and, 31º, tested at five collective pitches; 14.4º, 28.8º, 43.2º, 57.6 º, and 72º. The trends of the results match those expected by Brindejonc *et al.*; the Thrust vs. Descent Velocity data was parabolic for each blade configuration and the RPM vs Descent Velocity was linear. It was found that the highest thrust for each blade twist was achieved at the lowest possible collective pitch. For

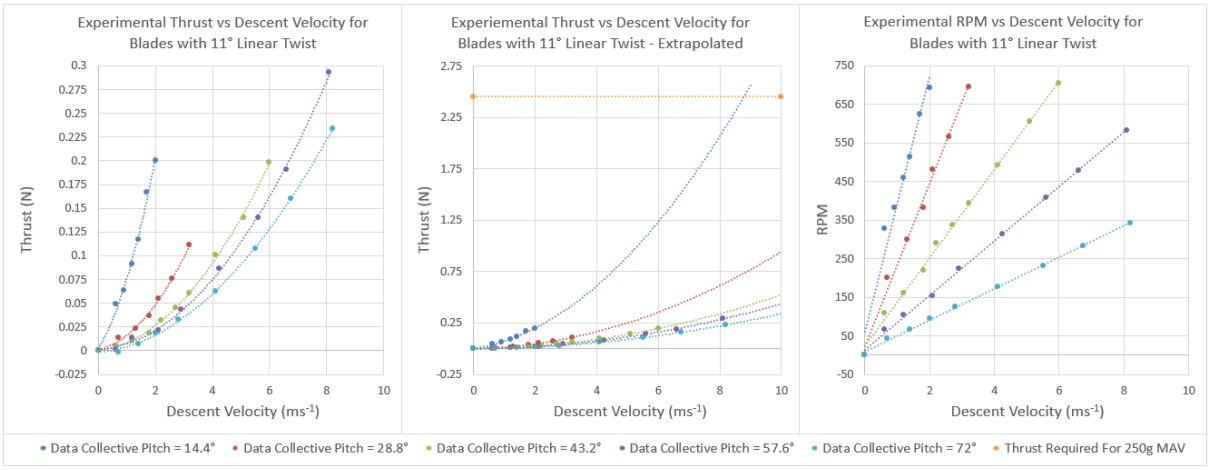

Figure 13. Initial Experimental Data for Blades with Linear Twist of 11 Degrees

twists 0º – 19.5º this collective pitch was 14.5º however for twists for 25º and 31º , 14.5º collective pitch failed to provide the geometry required to initiate the correct direction of rotation. As noted by Brindejonc *et al.* the blades must have a negative geometric pitch between the blade root and three quarters of the rotor disc radius in order to initiate rotation in the desired direction. Thus the lowest achievable collective pitch for blades of 25º and 31º twist was 28.8º. Fig.13 displays the results from the testing of blades with 11º twist at the five collective pitches. These results, which are indicative of the behaviour of all the blade twists tested, show that as collective pitch is reduced both the thrust and rotational speed increase. The result of these relationships was that very little data was obtained for the configurations which showed the most promise in terms of thrust production. Subsequently considerable extrapolation was required to gain meaningful data however this meant that the data was susceptible to substantial mathematical error.

Once the initial data had been collected and analysed a second set of tests were conducted. Having shown that low collective pitches produced the most thrust the second set of tests were conducted only at a collective pitch of 14.4º with blades of 0º, 11º, 16º, 19.5º twist to gain more data at the point of highest interest.

The experimental results, displayed in Fig.14 and Table.1 showed that twisting the blades could markedly improve the autorotation performance. To compare the results the thrust required to support a 250 g MAV was calculated, the descent rate required to achieve this force was then identified for each of the blade twists. It was found that blades with a twist of 16º could reduce the descent rate to 6.43 ms^{-1} compared to the12.23 ms^{-1} achieved by untwisted blades. It should be noted however that 16º is most likely not the optimum value as the experimental resolution was not high enough to prove that 16º was preferable to the other values that lie between 11º and 19.5º. In order to more specifically identify the optimum value for blade twist it would be necessary to further increase the resolution of the experiment.

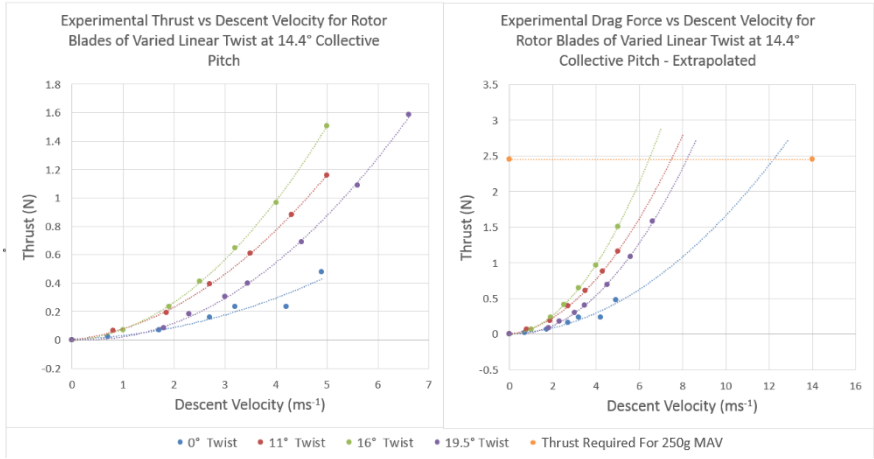

Figure 14. Complete Experimental Data for Blades with Varied Linear Twists at 14.4 Degrees Collective Pitch

E. Computational Analysis Results

The computational analysis provided data which conformed to the expected trends of parabolic thrust vs descent rate and linear RPM vs descent rate however was unable to identify accurately the effects of blade twist.

The raw computational data was susceptible to unpredictable fluctuations and resultant outliers. These outliers tended to be more frequent as blade twist was increased and appeared to be affected by the lift curve slope used to calculate the aerodynamic coefficients. It is most likely that fluctuations were the result of the simulation not being able to converge the aerodynamic values during the BEMT portion of the code, this is discussed by Brindejonc *et al.* as being a complication in a similar computational method [4]. The most consistent results were gained where [13]:

$$C_d = 2(\sin\alpha)^2 \qquad (17)$$

And;

For $-15° \leq \alpha \geq 15°$

$$C_l = 2\pi\alpha \qquad (18)$$

For $\alpha < -15° \ or \ 15° < \alpha$

$$C_l = 2\sin\alpha\cos\alpha \qquad (19)$$

Twist		C_T	C_T Difference (%)	V_d (250g) (ms-1)	V_d Difference (%)
0°	Experimental	0.118	39.44	12.228	-19.37
	Computational	0.164		9.860	
11°	Experimental	0.293	34.23	7.474	-17.62
	Computational	0.393		6.157	
16°	Experimental	0.372	48.41	6.434	-21.17
	Computational	0.552		5.072	
19.5°	Experimental	0.192	253.45	8.206	-44.88
	Computational	0.679		4.523	

Table 1. Results Summary of Computational and Experimental Analysis of Linearly Twisted Blades at 14.4° Collective Pitch During Steady Autorotation

Once the outliers were manually removed from the computational data the experimental and computational results for 0º, 11º, 16º and 19.5º blade twist at 14.4º collective pitch were compared. The results of this comparison is displayed in Tab.1 and Fig.15. The same method used to predict the descent speed of a 250 g projectile was used to quantify the performance predicted by the computational analysis. Additionally the coefficient of thrust was taken for both the computational and the experimental data using the following equation;

$$C_T = \frac{T}{2\rho A V^2} \qquad (20)$$

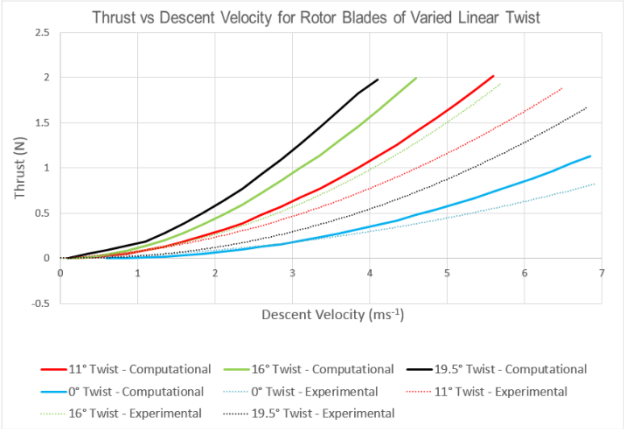

Figure 15. Comparison of Computational and Experimental Results

Through comparison of the data produced by the experiment and the computational analysis it became evident that the computational analysis predicts higher performance than that which was achieved in experimentation. This difference, at first glance could be attributed purely to physical loses in the test environment such as rolling resistance, aerodynamic loses due to the three dimensional nature of the physical blades and aerodynamic interaction of the model with the wind tunnel environment. However it also becomes clear that the trends produced by the computational analysis are also dissimilar to that produced in experimentation. The computational analysis fails to recognise the peak in autorotation performance between 11º and 19.5º twist as identified by the experimental analysis. It can therefore be concluded that the computational analysis is not yet complete enough to be considered practical for predicting autorotation performance.

B. Concurrent Work

A. Development and Testing of Initiator

In parallel with this project further developments in the design of the initiator were made. Following on from Rolph, Stockdale redesigned and produced an aluminium prototype of the initiator and subsequently test firings were conducted using blank projectiles at the Graytown Experimental Range in Victoria. The testing found that the free piston trigger system implemented was effective in providing instantaneous propulsive pressure to the projectile with minimal ramp up and that the exit velocity produced was within 10% of that predicted by computational analysis. The testing also displayed the significant effects of unstable flight on the projectile's trajectory. The rudimentary projectiles used during the testing of the initiation system tended to tumble during their ballistic flight, producing increased drag forces and significant reductions in achieved altitude. This instability was likely caused by imperfections in the projectile's centre of mass and will need to be addressed in future work on the project.

C. Future work

A. Blade Element Momentum Theory Simulation Correction

It is evident from the results that the comparison between the computational analysis and experimental results that the computational analysis is not yet capable of accurately predicting the performance of the descending MAV. During ideal autorotation highly loaded sections of the rotor blades enter VRS defined by $\frac{V_c}{V_h} \geq -2$. VRS produces unpredictable airflow and us such invalidates BEMT [4,5,6,17,22]. In order to prevent VRS from having a detrimental effect on the established simulation it will be necessary to make changes to the simulation so that VRS is not reached. This will involve the implementation of controls within the simulation which recognise where VRS is reached and subsequently initiate the extrapolation of data produced by the lower RPM values analysed prior to VRS being encountered.

B. Further Wind Tunnel Testing

The combinations of blade parameters available to the MAV are effectively limitless. Thus far the effects of chord, length, pitch and twist have been investigated however there remains a significant number of further characteristics which stand to improve the performance of the descending MAV. Pre-cone and pitch-flap angle as well as radially variable chord and airfoil profile optimisation all stand to further improve performance of the descending MAV however it is evident that finding the ultimate combination of blade properties would be a very complex task. As such it is recommended that further investigation into blade design is not prioritised over the conduct of the tasks required to prove that the MAV concept is fundamentally feasible.

C. Development of Stable Ballistic Flight and Transition

To date the MAV's initiation and descent have been proven to be achievable however for the system to operate effectively the projectile must be capable of maintaining stable flight during its ballistic stage and subsequently transitioning into autorotation. Stabilisation is likely to be difficult to achieve relying on mass distribution alone, as such thought needs to be allocated to the installation of fins or to the integration of rifling. Once a stable trajectory is attained work must be conducted on the transitional stage. Geometrically two options are available, the mounting of the rotor hub at the rear of the projectile or toward the nose. The transition profiles for these two arrangements are described by Fig.16. Mounting the blades toward the nose would require the projectile to reverse its flight direction however provides the opportunity to use the reversed airflow to passively deploy the rotor blades. Mounting the blades at the rear of the projectile allows the craft to follow its natural trajectory and subsequently utilise its pre-existing motion to spin up the rotor blades, however an active blade release system would be required to initiate the transition. An active release system could be triggered by a timer similar to those in parachute flares, an altimeter or an inertial measurement unit.

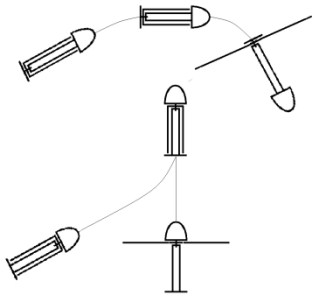

Figure 16. Transition Profiles

D. Conclusions

This project has conducted wind tunnel experimentation to test the effects of blade twist on passive autorotation performance as well as developing the initial structure of a computational autorotation model using BEMT and RPM Sweep. This study has shown that a 250 g autorotating MAV operating with a negative collective pitch of 14.4^{o} could have its descent rate decreased by up to 47% through implementing positive blade twist of between 11^{o} and 19.5^{o}. This reduction in descent speed benefits the Falling Spy Project by increasing the amount of time that the MAV is airborne and consequently increasing the quantity of information provided to its operators. Additionally the experimental data collected provides the means to verify future computational models developed for Project Falling Spy and the wind tunnel model and processes developed provide the experimental means to further optimise the Falling Spy in the future. The computational model forms the basic structure of a autorotation performance analyser however before it becomes practical further developments must be made in order to compensate for VRS, three dimensional losses and convergence errors.

Acknowledgements

The author would like to acknowledge Dr. Sean O'Byrne for his guidance and assistance with the project and to Mr. Paul Walsh for generously providing his time and extensive technical expertise. Acknowledgements are also given to Sub Lieutenant Timothy Laughlan and Pilot Officers Samuel Stockdale and Scott Johnson for their assistance during the project and to the members of the 2014 Space Panel for their cooperation, advice and input.

References

[1] Aeronautical, G. A. (2014). *Predator® UAS*. Retrieved May 2014, from General Atomics Aeronautical: http://www.ga-asi.com/products/aircraft/predator.php

[2] Aerovironment. (2014). *UAS: Dragon Eye.* Retrieved May 2014, from Aerovironment: http://www.avinc.com/uas/small_uas/dragon_eye/

[3] Aerovironment. (2014). *UAS: Wasp.* Retrieved May 2014, from Aerovironment: https://www.avinc.com/uas/small_uas/wasp/

[4] Brindejonc, A., Jayant, S., & Chopra, I. (2005). *Design and Testing of an Autorotative Payload Delivery System: The Autobody.* University of Maryland: Alfred Gessow Rotocraft Center, Dpeartment of Aerospace Engineering.

[5] Cuerva, A., Sanz-Andres, A., Maseguer, J., & Espino, J. (2006). An Engineering Modification of the Blade Element Momentum Equation for Vertical Descent: Fundamentals and Validation. *Journal of the American Helicopter Society*, 341-348.

[6] Cuerva, A., Sanz-Andres, A., Meseguer, J., & Espino, J. (2006). An Engineering Modification of the Blade Element Momentum Equation for Vertical Descent: An Autorototaion Case Study. *Journal of the American Helicopter Society*.

[7] Dreier, M. (2007). *Introduction to Helicopter and Tilt Rotor Flight Simulation.* AIAA: Blacksburg.

[8] Dynamics, P. (2014). *PD-100 Black Hornet*. Retrieved from Proxy Dynamics: http://www.proxdynamics.com/products/pd-100-black-hornet

[9] Gnemmi, P., & Haertig, J. (2008). Concept of a Gun Launched Micro Air Vehicle. *26th AIAA Applied Aerodynamics Conference.* Honolulu: AIAA.

[10] Grasmeyer, J., & Keenon, M. (2001). *Development of the Black Widow Micro Air Vehicle.* Simi Valley: Aerovironment.

[11] Grumman, N. (2014). *Global Hawk*. Retrieved May 2014, from Northrop Grumman: http://www.northropgrumman.com/capabilities/globalhawk/Pages/default.aspx

[12] Gundtoft, S. (2009). *Wind Turbines.* Århus: University College of Århus.

[13] Hoerner, S. (1985). *Fluid Dynamic Lift.* Hoerner.

[14] Johnson, W. (1994). *Helicopter Theory.* New York: Dover Publications.

[15] Kelderman, T. (2013). *Project Falling Spy.* Canberra: UNSW.

[16] Laughlan, T. (2014). *A Numerical and Experimental investigation of a Gurney Flap on a Newman Airfoil.* Canberra: UNSW.

[17] Leishman, J. (2000). *Principles of Helicopter Aerodynamics.* Cambridge: Press Syndicate of the University of Cambridge.

[18]Liu, S., & Janajreh, I. (2012). Development and application of an improved blade element momentum method model on horizontal axis wind turbines. *International Journal of Energy and Environmental Engineering*, 1-10.

[19]Moriarty, P., & Hansen, A. (2005). *AeroDyn Thoery Manual.* Golden: National Renewable Energy Laboratory.

[20]Mueller, T. (2006). *Overview of Micro-Air-Vehicle Development.* Indiana: University of Notre Dame.

[21]Murphy, S., & Mullen, M. (2005). *Aerial Canopy Sensor Delivery System (ACSDS) for Lightweight Payload Deployment Applications.* Manassas: Progeny Systems Corporation.

[22]Padfield, G. (2007). *Helicopter Flight Dynamics.* Washington: AIAA.

[23]Palmeri, F. (2003). *Model Helicopter Tail Rotor Simulation.* Canberra: UNSW.

[24]Pope, A., & Harper, J. (1966). *Low Speed Wind Tunnel Testing.* New York: John Wiley & Sons, Inc.

[25]Power, N. (2012). *Design and Modelling of a Disposable Micro Air Vehicle using Autorotation.* Canberra: UNSW.

[26]Rayner, S. (2002). *Further Investigation of the Gurney flap.* Canberra: UNSW.

[27]Rolph, P. (2013). *Feasibility Study of a Lightweight and Disposable Information, Surveillance and Reconnaissance Solution for Tactical Environments.* Canberra: UNSW.

[28]Samad, T., Bay, J., & Godbole, D. (2007, January). Network-Centric Systems for Military Operations in Urban Terrain: The Role of UAVs. *Proceedings of the IEEE*, pp. 92-107.

[29]Schechter, E. (2013, November 03). *Palm-Size Drones Buzz Over Battlefield*. Retrieved May 10, 2014, from Live Science: http://www.livescience.com/40908-palm-size-drones-buzz-over-battlefield.html

[30]Stockdale, S. (2014). *Design, Analysis and Validation of a Tactical Surveillance Launch System.* Canberra: UNSW.

[31]USAF. (2009). *U.S. Air Force Fact Sheet RQ-11B Raven System.* Hurlburt Field: Air Force Spoecial Operations Command.